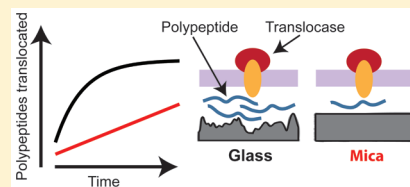


Protein Translocation Activity in Surface-Supported Lipid Bilayers

Kanokporn Chattrakun,[†] David P. Hoogerheide,^{‡,§} Chunfeng Mao,[§] Linda L. Randall,[§] and Gavin M. King^{*,†,§}[†]Department of Physics and Astronomy, and [§]Department of Biochemistry, University of Missouri-Columbia, Columbia, Missouri 65211, United States[‡]Center for Neutron Research, National Institute of Standards and Technology, Gaithersburg, Maryland 20899, United States

Supporting Information

ABSTRACT: Surface-supported lipid bilayers are used widely throughout the nanoscience community as cellular membrane mimics. For example, they are frequently employed in single-molecule atomic force microscopy (AFM) studies to shed light on membrane protein conformational dynamics and folding. However, in AFM as well as in other surface-sensing techniques, the close proximity of the supporting surface raises questions about preservation of the biochemical activity. Employing the model translocase from the general secretory (Sec) system of *Escherichia coli*, here we quantify the activity via two biochemical assays in surface-supported bilayers. The first assesses ATP hydrolysis and the second assesses polypeptide translocation across the membrane via protection from added protease. Hydrolysis assays revealed distinct levels of activation ranging from medium (translocase-activated) to high (translocation-associated) that were similar to traditional solution experiments and further identified an adenosine triphosphatase population exhibiting characteristics of conformational hysteresis. Translocation assays revealed turnover numbers that were comparable to solution but with a 10-fold reduction in apparent rate constant. Despite differences in kinetics, the chemomechanical coupling (ATP hydrolyzed per residue translocated) only varied twofold on glass compared to solution. The activity changed with the topographic complexity of the underlying surface. Rough glass coverslips were favored over atomically flat mica, likely due to differences in frictional coupling between the translocating polypeptide and surface. Neutron reflectometry and AFM corroborated the biochemical measurements and provided structural characterization of the submembrane space and upper surface of the bilayer. Overall, the translocation activity was maintained for the surface-adsorbed Sec system, albeit with a slower rate-limiting step. More generally, polypeptide translocation activity measurements yield valuable quantitative metrics to assess the local environment about surface-supported lipid bilayers.



INTRODUCTION

Many proteins in living cells need to be transported across membranes to properly localize and function. Different pathways have evolved to accomplish this complex task. Among protein export pathways, the general secretory system (Sec) is ubiquitous, having homologues across all domains of life. In *Escherichia coli*, the general secretory system comprises a translocase consisting of SecA, a peripheral membrane adenosine triphosphatase (ATPase), in complex with an integral membrane translocon, SecYEG.¹ The translocon exhibits a protein conducting channel with dimensions capable of passing polypeptides through the cytoplasmic membrane. Proteins destined for the Sec pathway are produced at the ribosome as precursors with a signal sequence. The Sec system cannot translocate precursor proteins with a stable tertiary structure.^{2,3} One role of the signal, an amino-terminal extension of the mature protein sequence, is to often allow the chaperone SecB to capture the precursor before it folds. In a highly dynamic ATP-dependent process that is only superficially understood, the precursor is passed from SecB to SecA and then through the membrane via SecYEG.

SecA plays a central role in orchestrating translocation. In addition to harvesting the energy generated from ATP

hydrolysis, it has many binding partners: precursor proteins, SecB, lipid bilayers, and SecYEG.^{1,2} Structures of SecA and other Sec system components have been obtained at high resolution and have significantly advanced the field. However, the inherent complexity and dynamic interplay among components of the system have left central questions unanswered, including the nature of the translocation step itself. Evidence of power stroke, Brownian ratchet, and other mechanisms has been reported.^{1,2,4,5} Direct observation of conformations and conformational dynamics of active translocases could help resolve the ongoing debate. Such observations are made possible through single-molecule methodology, which relaxes the requirement of ensemble averaging. Though technically challenging, single-molecule investigations of the Sec system have begun in earnest and have provided insights inaccessible to traditional biochemical methods.^{6–15}

The atomic force microscope (AFM) is a powerful single-molecule tool that is capable of visualizing dynamic

Received: June 25, 2019

Revised: August 14, 2019

Published: August 25, 2019

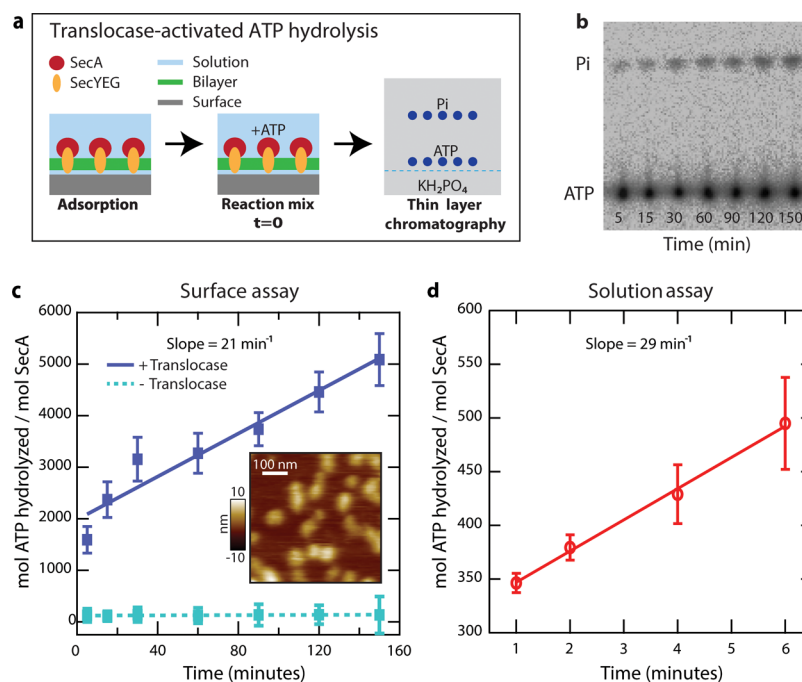


Figure 1. Surface ATP hydrolysis assay and comparison with solution assay. (a) Cartoon of translocase-activated ATP hydrolysis assay. Proteoliposomes YEG-A were adsorbed onto the surface. After rinsing (*not drawn*), radiolabeled ATP was added. At subsequent times, the solution above the membrane surface was analyzed via TLC. (b) Image of TLC plate showing the generation of ^{32}P i from ATP over time. (c) Plot showing the amount of ATP hydrolyzed normalized to the amount of SecA available as a function of time. A control trace without proteoliposomes YEG-A is also shown (dashed). Inset: AFM image of YEG-A protrusions. (d) Solution assay results with proteoliposomes YEG-A. Rates were calculated from slopes of linear fits, and error bars are SD ($N = 3$).

conformations of individual membrane proteins with ~ 1 Å vertical (normal to the membrane surface) and ~ 1 nm lateral resolution.¹⁶ AFM has been utilized to study Sec system components in isolation as well as in supported lipid bilayers.^{7,10,12,15,17,18} The advantages which AFM provides include the ability to monitor conformational dynamics in solution without the need for additional labeling. However, the technique requires that the specimens be adsorbed to a supporting surface, though bilayer stacking, tethering, or other cushioning methods have been developed to modulate the submembrane space.^{19–22}

Regardless of the bilayer preparation method employed, there is a need for quantitative activity benchmarks. Questions about the preservation of biochemical activity in surface-supported systems, and hence biological relevance, often arise. For example, to make progress in understanding the Sec system via AFM or other precision surface-coupled single-molecule assays,²³ it is important to determine if the biochemical activity of the system is altered by proximity to the underlying solid-state surface. Additionally, once established, translocation activity can be used as a metric to quantitatively compare and to optimize supported lipid bilayer systems.

Through the years there have been attempts to verify that surface-adsorbed proteins retain biochemical activity.^{24–33} Early in the field of biological AFM investigation, transient deflections of cantilevers positioned above surface-adsorbed lysozymes were reported to result from enzymatic turn over, though following this strategy is challenging due to low frequency instrumental noise (i.e., tip-sample drift).²⁴ More recently, evidence of activity has come from direct imaging of motor proteins “walking” along cytoskeletal tracks,^{30,31} though this approach can only be applied to a limited set of motile

proteins. Hence, several methods have been used to probe the activity of surface-adsorbed proteins, but have exhibited varying degrees of success and generality.

Here, we demonstrate protein translocation activity in surface-supported lipid bilayers and deduce chemomechanical coupling (ATP hydrolyzed per residue translocated) in a surface-dependent manner. Two biochemical assays were used to verify activity of the surface-adsorbed Sec system prepared for precision surface-coupled measurements such as AFM.^{10,12} The methods were adopted from highly sensitive techniques that monitor separate aspects of the chemomechanical reaction underlying Sec system function.^{2,34} To probe the ATPase activity, we tracked dephosphorylation of radioactive [γ - ^{32}P] ATP. Different levels of the hydrolysis activity were found to be distinguishable with the method. Interestingly, SecA that was released from membrane-bound translocases remained in a highly activated state, rapidly hydrolyzing ATP for extended time periods, suggestive of conformational hysteresis. To probe translocation activity, we followed the protection of radiolabeled precursor proteins from degradation by an added protease. Two surfaces were utilized: freshly cleaved mica and cleaned borosilicate glass coverslips. Glass-supported Sec translocases exhibited a substantial enhancement in translocation activity compared to mica. This may be attributable to the topographic asperities of glass providing more space for the precursor to occupy. Neutron reflectometry (NR) on a closely related silicon oxide surface provided submembrane information and corroborated the biochemical results.³⁵ Two translocating polypeptide species were employed, the precursor of outer membrane protein A (pOmpA) and the precursor of galactose-binding protein (pGBP). The data revealed that the hallmark of the Sec system activity is preserved in mica- or glass-supported translocases: ATP-dependent precursor pro-

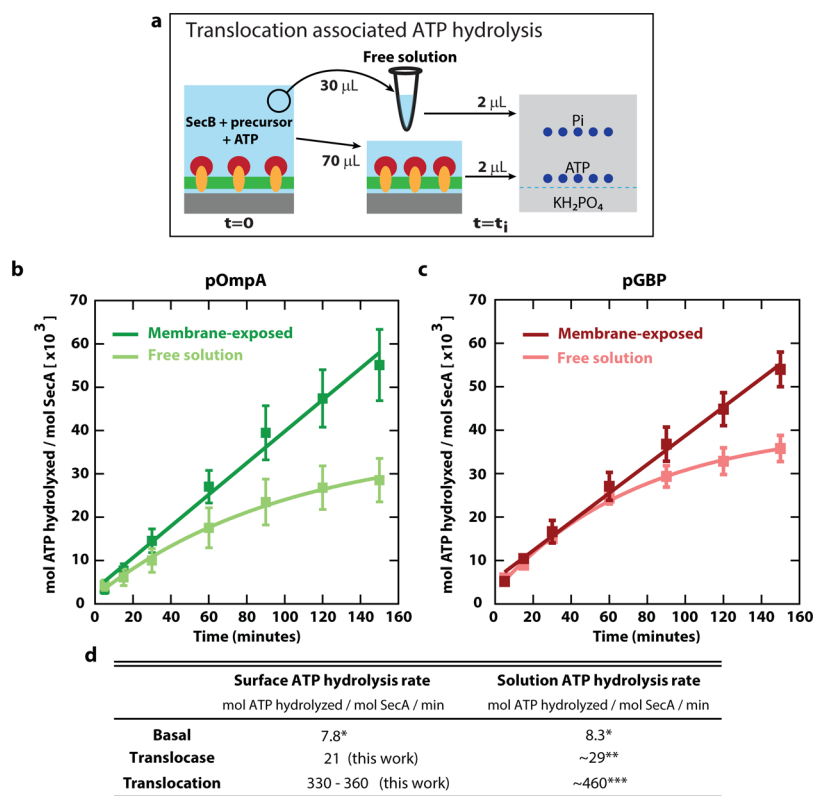


Figure 2. Translocation-associated ATP hydrolysis assay. (a) Proteoliposomes YEG-A were adsorbed on mica and rinsed. A solution containing SecB, precursor protein (pOmpA or pGBP), and radiolabeled ATP was added. Immediately thereafter, 30 μL of solution was transferred to a separate tube (free solution). At subsequent times, solutions were sampled, mixed with EDTA to stop the reaction, and analyzed via TLC. (b) Plot of ATP hydrolyzed as a function of time with pOmpA from the membrane-exposed solution (dark green) and free solution (light green). (c) Analogous plot with pGBP for the membrane-exposed solution (dark red) and free solution (light red). Data normalized to mol SecA available, error bars are SD, $N = 3$. The hydrolysis rates in the membrane-exposed solutions were 364 and 330 min^{-1} for pOmpA and pGBP, respectively. (d) Table comparing ATP hydrolysis activities on mica vs in solution, data from refs (10)*, (37, 38)***, and (34, 36, 37)***.

tection. Results were compared to assays carried out in solution wherein the translocons can be taken to be in a native environment.

RESULTS AND DISCUSSION

ATP Hydrolysis I: Translocase-Activated. We measured the ATP hydrolysis activity emanating from surface-supported translocase complexes. The sample material comprised proteoliposomes SecYEG coassembled with SecA (YEG-A) using *E. coli* polar lipids (see Materials and Methods for details).¹⁷ This system reflects the activity of SecYEG in its native environment and is significantly enhanced compared to the standard reconstitution system wherein SecA is added subsequently to SecYEG proteoliposomes (YEG + A).³⁶ The approach extends our previous work in which we monitored the activity of SecA alone, that is, in the absence of any lipid or other binding partners. SecA adsorbed onto mica alone exhibited the expected basal level of hydrolysis, achieving an activity level very close to (>90%) that measured in solution.¹⁰ However, SecA in complex with SecYEG hydrolyzes ATP at a substantially higher rate than SecA alone, and the presence of lipids can also alter the activity.^{8,37}

To evaluate these effects, we developed a surface-based translocase-activated ATP hydrolysis assay (Figure 1a). As in AFM imaging protocols, proteoliposomes YEG-A were first incubated on freshly cleaved mica. During this time, the liposomes adsorbed to the surface and fused together, forming two dimensional supported lipid bilayers over large areas with

few defects or voids.¹² Incubation was followed by rinsing to remove loosely bound materials. Then, a reaction solution containing radioactive ATP was added. At selected times, the solution above the membrane surface was sampled, added to a solution containing EDTA to stop the reaction, and spotted on a plate subject to thin-layer chromatography (TLC). The radioactivity on the dried plate was quantified using a phosphor imager (Figure 1b). The percent ATP hydrolyzed was converted to mol ATP hydrolyzed per mol SecA and plotted versus time (Figure 1c). We estimated the amount of translocons containing SecA accessible on the surface, ~ 0.03 pmol, using the dimensions of the mica disk (~ 300 mm²) and the density of translocase protrusions observed in AFM images.¹² A representative AFM image of YEG-A is shown (Figure 1c, inset). The plot of mol ATP hydrolyzed per mol SecA versus time exhibited a slope of (20.9 ± 2.5) min^{-1} . Errors are 68% confidence intervals (CI) from least squares fits to the data, $N = 3$. This value can be compared with a traditional assay carried out with the same YEG-A sample in solution (Figure 1d). Translocase-activated ATP hydrolysis on mica achieved a rate that was $\sim 72\%$ of the solution assay (29.1 ± 1.3) min^{-1} , $N = 3$. In addition to close overall agreement with solution assays, the results also show that translocase-activated ATP hydrolysis persisted over a time period of >1 h. This timescale is commensurate with that of typical single-molecule studies.

ATP Hydrolysis II: Translocation-Associated. The highest level of ATP hydrolysis activity is expected when

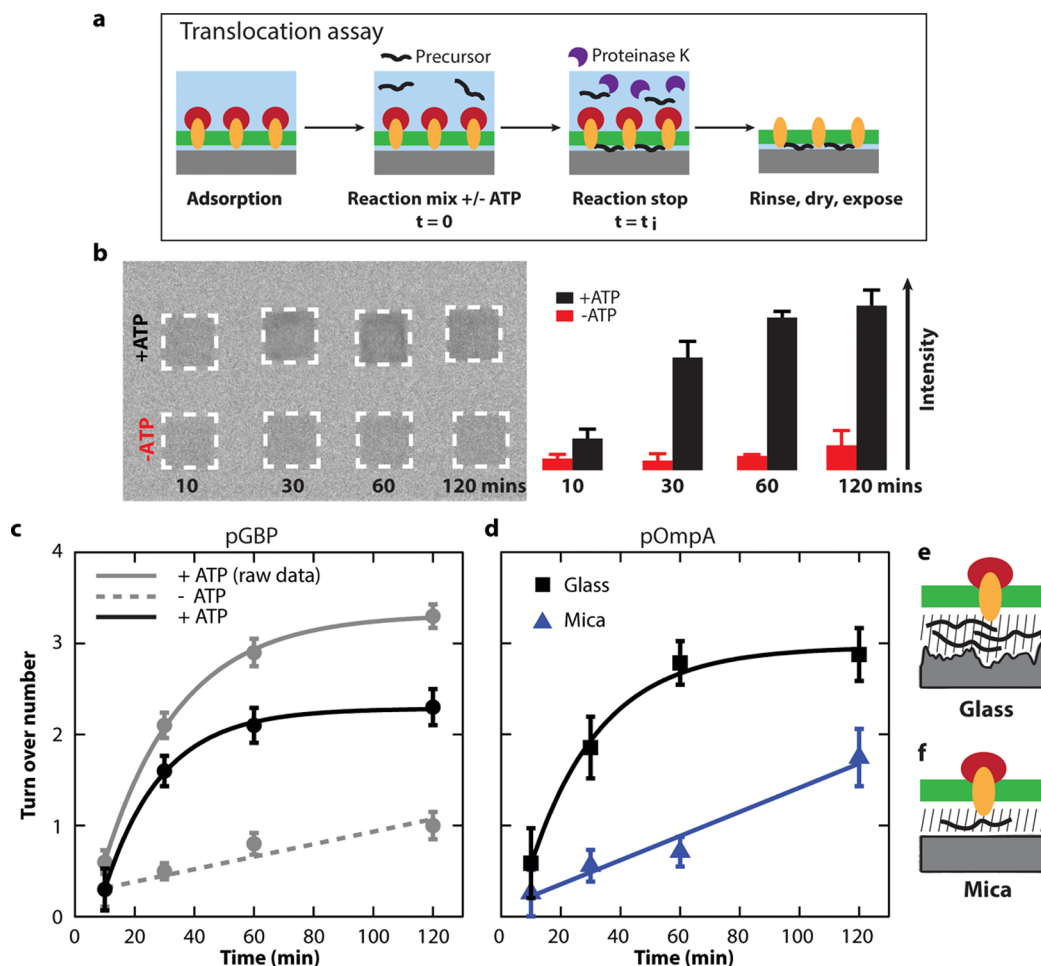


Figure 3. Surface translocation activity assay. (a) Schematic of surface translocation activity assay which quantifies the amount of radiolabeled precursor protein (blue) protected \pm ATP. (b) Phosphor image of glass surfaces at indicated times. The location of the glass is highlighted (dashed squares). The intensity of protected pOmpA was quantified and shown in bar graphs (+ATP, black; -ATP, red). (c) Turn over number (mol precursor protected per mol translocase accessible) is plotted as a function of time for pGBP on glass coverslips. Raw data (gray solid line) as well as data from which the -ATP background was subtracted (black solid line) are shown. (d) Background subtracted plots for pOmpA on glass (black squares) or mica (blue triangles). Error bars are SD ($N = 3$). (e,f) Cartoons (not to scale) showing how the rougher underlying topography of glass could create space that enhances translocation activity in comparison to mica.

precursor proteins and SecB are added to proteoliposomes YEG·A.³⁸ This forms a full system with activity levels comparable to SecYEG in a native environment, inner membrane vesicles, after accounting for the fraction of accessible translocons, the orientations of which are randomized during reconstitution.^{17,36,37} To demonstrate enhanced activity during translocation, we included precursor proteins and chaperone SecB (which minimizes premature precursor folding) to the surface ATP hydrolysis assay (Figure 2a). Two precursor species were employed: pOmpA and pGBP. TLC analysis was carried out as described above.

Translocation-associated ATP hydrolysis data for translocation of pOmpA and pGBP in mica-supported lipid bilayers are shown (Figure 2b,c, respectively). The slope of these curves represents the rate at which inorganic phosphate (Pi) was released from ATP, normalized to the estimated amount of SecA available to participate in the reaction. As expected, the difference between ATPase rates with each precursor was minimal.³⁶ The translocation-associated ATP hydrolysis rate with pOmpA was $(364 \pm 17) \text{ min}^{-1}$ while the rate with pGBP was $(330 \pm 11) \text{ min}^{-1}$. For both precursors, the translocation-associated rate was more than an order of magnitude higher

than the translocase-activated rate and >40-fold higher than the basal ATP hydrolysis rate that we previously measured for SecA alone.¹⁰

It is informative to compare ATPase rates to those measured in traditional solution-based assays.^{34,36–38} As shown in the table (Figure 2d), the hydrolysis rates under all levels of activation are comparable to those observed in traditional assays. In particular, the translocase-activated and translocation-associated rates were >70% of the solution rates. The overall agreement between these assays implies that the majority of accessible YEG·A complexes remain competent for ATP hydrolysis and release Pi at a rate similar to that achieved in solution. Additionally, despite the small number of translocase units participating, the surface-based assay we employ here has sufficient sensitivity to distinguish different levels of ATP hydrolysis.

As a peripheral ATPase, SecA is known to dissociate from the membrane during translocation^{1,12,39} and this population of SecA should continue to hydrolyze ATP, but at what level? To evaluate this, immediately after adding radiolabeled ATP, a 30 μL volume of solution above the mica surface (Figure 2a, free solution) was moved to a microcentrifuge tube for

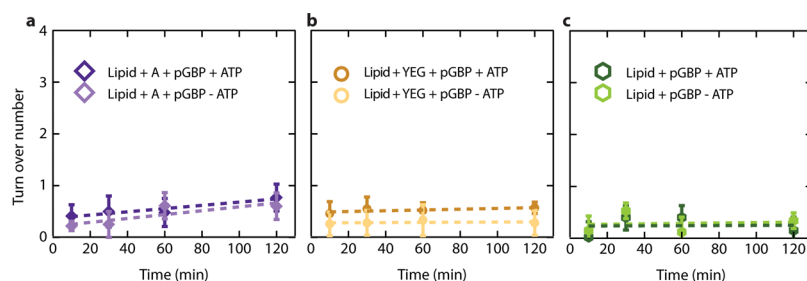


Figure 4. Both SecYEG and SecA are required for translocation activity. Assays carried out on glass surfaces with all of the required components of the general Sec system excepting SecYEG (a), SecA (b), or (c) both SecYEG and SecA. All experiments show minimal translocation as evidenced by the lack of ATP-dependent protection of precursor pGBP. Best fit lines (dashed) are shown, error bars are SD ($N = 3$).

quantification in parallel with the membrane-exposed volume. Surprisingly, the free solution data for both precursor species exhibited highly activated hydrolysis levels for extended time periods [Figure 2b,c, light green (pOmpA) and light red (pGBP)]. This population of SecA had been exposed to the full Sec system for ~ 1 min before being separated from the membrane-bound SecYEG; yet, the hydrolysis rates essentially matched the translocation-associated rates for tens of minutes before decreasing. We note that surface-adsorbed samples were rinsed extensively prior to beginning the assay; thus, it is not likely that SecYEG detached from the surface during the assay. Further, exposure of SecA to precursor protein, which is likely in the free solution in the absence of SecYEG, does not activate SecA ATP hydrolysis.³⁷ This SecA activation was independent of the substrate surface species. Samples supported by glass coverslips showed similar hydrolysis activities to mica-supported samples in both the free solution as well as in the membrane-exposed volumes (Supporting Information Figures S1 and S2). As demonstrated here, surface-based activity assays allow straightforward separation between membrane-exposed fractions and free solution fractions. This can be viewed as a general advantage of such assays.

Translocation Activity: Probing Precursor Protection.

The coupling between chemical energy consumed (ATP hydrolysis) and work done moving polypeptides across the membrane is not tight in the Sec system and has been shown to vary with precursor species.³⁶ Hence, to complement ATP hydrolysis measurements, we developed a surface-based translocation activity assay that tracked the protection of precursor proteins in an ATP-dependent manner.^{12,40} Translocation is demonstrated on two distinct supporting surfaces. We compare results using mica, which is atomically flat over large areas, to cleaned borosilicate glass coverslips, which exhibit topographic asperities that may provide additional submembrane space for the precursor to occupy.¹⁸

Because proteinase K does not cross the lipid bilayer, translocation can be inferred via protection of radiolabeled precursors from proteinase activity above the membrane surface (Figure 3a).⁴⁰ Proteoliposomes YEG·A were adsorbed onto either freshly cleaned glass coverslips or freshly cleaved mica surfaces, creating supported lipid bilayers over large areas.¹⁸ After rinsing to remove the loosely adsorbed material, a reaction mixture containing SecA, SecB, and radiolabeled precursor (pOmpA or pGBP) was added in the presence and absence of ATP. At predetermined times, surfaces were treated with urea (a denaturing agent) to destabilize the proteins and render them sensitive to proteolysis by added proteinase K. Finally, surfaces were rinsed, dried, and exposed to a phosphor imaging plate for analysis.

The amount of radioactivity exhibited by the protease-treated membrane was quantified. Figure 3b shows data for pOmpA on borosilicate glass. The dashed squares highlight areas where the coverslips were placed on the imaging plate. The integrated intensity from the areas is shown in bar graphs on the right. The data (Figure 3b) show ATP-dependent precursor protection. This is the hallmark of active translocation. Analogous data for pOmpA on mica are shown (Supporting Information Figure S3). We created standard curves of pixel intensity as a function of mol radioactive precursor by spotting known quantities of precursor on surfaces (Supporting Information Figure S4). The calibration surfaces were dried and exposed to the imaging plate under identical conditions used to quantify translocation activity.

The turn over number versus time is plotted for pGBP and pOmpA on glass (Figure 3c,d, respectively). The vertical axis represents mol precursor protected per mol translocase accessible to precursors, that is, when added from above the glass surface, which is the same surface accessible to the AFM tip. The amount of translocase accessible was estimated to be 0.04 pmol which is slightly larger than the value for mica due to surface area differences. For both precursors, the translocation activity as a function of time exhibited similar exponential rise to maximum behavior, reaching a plateau between 2 and 3 translocation cycles with apparent rate constants of (0.052 ± 0.004) and (0.042 ± 0.009) min^{-1} for pGBP and pOmpA, respectively. Values were calculated after subtracting the $-$ ATP background, and errors are 68% CI estimated from non-linear least squares fits, $N = 3$. Apparent rate constants represent the rate constant of the slowest step in the cycle; more generally, they express the probability of a translocation event per unit time.

The translocation activity results varied significantly with the supporting surface (Figure 3d). With mica, the extent of translocation did not reach a plateau but was linear over the time tested. At 120 min, it was only $\sim 60\%$ of the glass result. The slope of the pOmpA turn over number versus time plot on mica was (0.013 ± 0.002) min^{-1} , $N = 3$, representing the mol pOmpA protected per minute normalized to the estimated mol translocase accessible on mica. This slope was fivefold lower than the initial slope on glass, which stayed approximately linear for 30 min before beginning to plateau (Figure 3d, compare black squares to dark blue triangles). These surface-dependent results may be attributable to distinctions in underlying topography. The cleaned borosilicate glass coverslips we utilized are approximately fivefold rougher than mica.¹⁸ Additional roughness likely leads to valleys in the submembrane space that precursors could move into, promoting more turn over events per unit time (Figure 3e,f). Additionally,

though both surfaces are highly hydrophilic, differences in surface chemistry and charge could also play a role. We posit that the lower effective rate constant observed on mica compared to glass is likely a result of a high level of confinement between the mica and the surface-proximal lower bilayer leaflet. Increased confinement produces a larger effective drag force on the translocating precursor, resisting motion.

Experiments were conducted to verify that the results observed reflect translocation activity through SecYEG. Both the translocon SecYEG and ATPase SecA were required to achieve active translocation in surface-supported assays. To show this, we probed the translocation activity of the full Sec system on glass, omitting either SecYEG (Figure 4a), SecA (Figure 4b), or both SecYEG and SecA (Figure 4c). As expected, in all three cases, no significant ATP-dependent protection of precursors was observed. As an additional control, we used AFM to image defects (noncomplete coverage) in the supported lipid bilayers, as changes in defect number or defect area with the addition of ATP could give rise to erroneous deductions of translocation. To generate defects for this experiment, surfaces were incubated for short periods (20 min). The data show no gross differences in bilayer defects \pm ATP (Supporting Information Figure S5); however, technical challenges associated with finding the same region of the surface before and after ATP addition make this experiment challenging to perform.

Comparisons of the extent of translocation (the maximal amplitude of the reaction) measured on glass coverslips to solution-based translocation assays using the same Sec system components are in close agreement (within a factor of two, determined by fitting the data to a single exponential rise to maximum, see Materials and Methods).³⁶ However, the apparent rate constants were reduced approximately 10-fold.³⁶ This rate constant reduction is likely due to an effective frictional drag force on the translocating precursor from the nearby solid-state surface.

To summarize, glass-supported YEG·A translocases maintain translocation activity, but with a slower rate-limiting step than solution-based assays. The same statement is true for translocases on mica surfaces, except that the rate-limiting step is even slower, presumably due to tighter submembrane confinement. It is not clear if the rate-limiting step observed on a surface is the same as that observed in solution. It is possible that a different step could become rate-limiting in surface-coupled assays compared to assays carried out in solution. The translocation activity persisted on both mica and glass surfaces for extended time periods (\sim 1 h).

Chemo-Mechanical Coupling. The energy provided by the hydrolysis of ATP is required for translocation of precursor proteins across the bilayer. Following the convention in the field that precursor protection comes about from transportation across the lipid bilayer,⁴⁰ the translocation-associated ATP hydrolysis and translocation activity assays were used to deduce chemomechanical coupling. On glass surfaces, we obtained chemomechanical coupling of approximately 13 and 15 ATP molecules hydrolyzed per amino acyl residue translocated for pGBP (332 residues) and pOmpA (346 residues), respectively. In solution assays with YEG·A as well as with inner membrane vesicles, which are taken to represent a native environment for SecYEG, these values are approximately 6 and 8 for pGBP and pOmpA, respectively.³⁶ Hence, the effect of adsorption onto glass caused an approximate 50%

change in chemomechanical coupling compared to solution assays. However, when YEG·A was adsorbed onto mica, a chemomechanical coupling value of approximately 80 was obtained for translocation of pOmpA. Therefore, fivefold more ATP was consumed per amino acyl residue translocated on mica compared to glass which may be attributed to tighter submembrane confinement on mica.

In the standard YEG + A reconstitution system used by many research groups, proteoliposomes are constructed from purified SecYEG, and then, SecA is added extraneously. YEG + A samples assayed in solution hydrolyze more ATP per residue translocated than do coassembled proteoliposomes YEG·A adsorbed to glass surfaces. In particular, the values for YEG + A in solution were 22 and 35 (ATP molecules hydrolyzed per amino acyl residue translocated) for pGBP and pOmpA, respectively.³⁶

Neutron Reflectometry. We characterized the submembrane structure of surface-adsorbed proteoliposomes YEG·A using NR. Because of instrumentation limitations, we could not utilize borosilicate glass coverslips nor mica in NR measurements. Here, proteoliposomes were incubated on a nominally 100 Å thick film of dry thermal silicon oxide (SiO_x) grown on a single crystal silicon wafer. SiO_x was chosen as a closely related surface proxy for borosilicate glass. However, these surfaces exhibit topographical and surface chemical differences that may alter behavior, for example, during proteoliposome rupturing and spreading (Supporting Information Figure S6). The sample wafer was mounted on a flow cell to allow subsequent buffer exchange. NR reflectograms were collected in both D_2O and H_2O -based buffers which mimicked the translocation activity buffers. Data from four conditions were used for analysis (Supporting Information Figure S7a).

NR data of the surface-adsorbed SecYEG-containing bilayer was analyzed using composition space modeling.⁴¹ The bilayer was assumed to consist of a single dioleoylphosphatidylcholine-like lipid species with an acyl chain volume of 1024 \AA^3 , a headgroup volume of 330 \AA^3 , an acyl chain scattering length of $-2.67 \times 10^{-4} \text{ \AA}$, and a headgroup scattering length of $6.00 \times 10^{-4} \text{ \AA}$. The bilayer was further assumed to contain SecYEG at the preparative molar fraction, which corresponds to about 7.6% in the hydrophobic region of the bilayer. The crystallographic structure of SecYEG (PDB ID: 3DIN)⁴² was used to generate the scattering length density (SLD) profile associated with the embedded protein. The orientation of the SecYEG in the membrane was taken to be equally distributed with the cytoplasmic protrusion exposed to the bulk solution (distal to the SiO_x surface) in 50% of total occurrences.¹⁷ For small bilayer-substrate separations, the submembrane space was too small to accommodate the extension of the SecYEG protein; in this region, the crystallographic SecYEG structure was truncated at the headgroup surface and evenly reallocated in the submembrane space so as to preserve the total protein volume. Peripheral SecA was modeled as a constant area fraction of protein extending from the headgroup surface.

Because of incomplete coverage of the proteoliposomes on the SiO_x surface, the data were modeled as the incoherent sum of the bilayer model and a second model in which significant areas ($>10 \mu\text{m}$)⁴³ of the substrate contain no liposomes. Nonspecifically adsorbed protein, which is likely to be SecA not bound to SecYEG, was modeled as a constant area fraction and density extending into the solution from the substrate surface. The fraction of the complete data set to be described by each model was allowed to vary in the optimizations. The

results of the model optimization (Supporting Information Figure S7a, solid lines) achieved a reduced χ^2 value of 1.41; the residuals are shown (Supporting Information Figure S7b). The SLD profiles corresponding to the two model regions (with and without the SecYEG-containing bilayer) are shown as solid and dashed (Supporting Information Figure S7c). Note that at distances from the substrate in which water is present, the SLD profile changes with the deuteration level of the buffer.

The individual molecular components are shown in Figure 5. The top 43% of the plot (Figure 5a, dashed lines) shows the

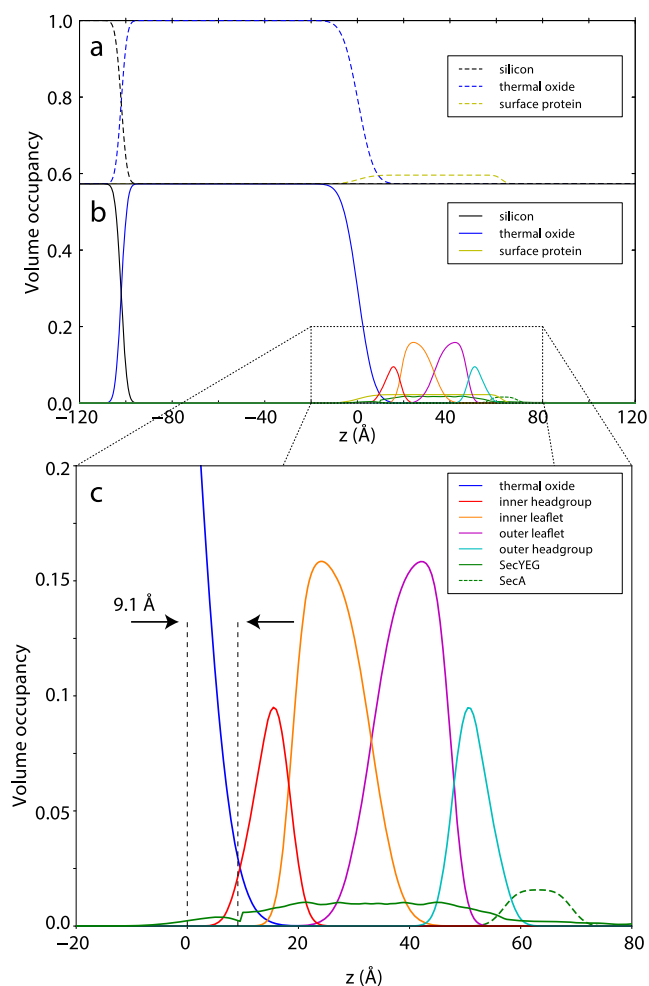


Figure 5. Neutron reflectivity reveals a submembrane structure of proteoliposomes YEG-A on SiO_x . (a,b) Results of the optimized underlying volume-occupancy model. Solid and dashed lines show the two model regions with and without adsorbed proteoliposomes, respectively. The solid line at 0.57 fractional occupancy reflects the relative weight of the two models determined in the optimizations. (c) Detailed view of the model in the vicinity of the SiO_x surface showing the 9.1 Å submembrane space.

structure of model region without proteoliposomes; the only molecular component is the nonspecifically adsorbed surface protein. The bottom 57% is the bilayer-containing region of the model (Figure 5b, solid lines), showing the two bilayer leaflets and the SecYEG. A complete list of fitting parameters and their optimized values is provided (Supporting Information Table S1). A detailed view of components at the bilayer/surface interface is shown (Figure 5c).

A principal quantity of relevance to this work is the average height of the submembrane space separating the SiO_x substrate from the headgroups of the substrate-proximal lipid leaflet, $9.1^{+0.5}_{-0.4}$ Å. More precisely this is defined as the distance from the center of the oxide/water interface to the center of the choline/water interface. Though relatively small, this amount of space is sufficient to accommodate precursor proteins. Unfolded protein segments exhibit very low bending stiffness. In particular, the submembrane space is more than double the 3.9 Å persistence length of an unfolded polypeptide, which itself is about the same as the size of a single amino acid, ~ 4 Å.⁴⁴ Additionally, 9.1 Å is equivalent to the radius of gyration of an approximately 10 amino acid long unfolded polypeptide (random coil) in free solution.⁴⁵ Other values of interest from the NR analysis include the total thickness of the bilayer (including headgroups), $48.5^{+1.0}_{-0.9}$ Å; the total separation of the top surface of the bilayer from the substrate, $57.5^{+1.0}_{-0.7}$ Å; and the total bilayer coverage, $15.9^{+0.7}_{-0.6}\%$. This last quantity is smaller than the bilayer coverage observed in AFM measurements on borosilicate glass. This could be due to topographical or surface chemical differences that alter proteoliposome spreading.⁴⁶

CONCLUSIONS

Sensitive activity assays quantified the biochemical integrity of model membrane protein complexes in surface-supported lipid bilayers. Both ATP hydrolysis assays as well as translocation activity assays confirmed the activity of the reconstituted Sec system in lipid bilayers supported by either mica or glass. Furthermore, surface-adsorbed translocases remained active for extended time periods (~ 1 h). This amount of time is commensurate with the typical data acquisition period of AFM experiments as well as with other precision single-molecule techniques such as optical trapping microscopy.

ATP hydrolysis assays revealed distinct levels of activity corresponding to previously defined levels in solution assays: basal (low), translocase-activated (medium), and translocation-associated (high). All of these levels were found to be similar to traditional solution assays (within $>70\%$). Interestingly, experiments identified a population of SecA that maintained a high level of ATP hydrolysis for tens of minutes despite being released from the membrane surface. This observation is suggestive of activation of SecA by a conformational change that slowly converts back to an unstimulated basal state.

Translocation assays on glass revealed the same exponential rise to maximum behavior observed in solution assays. Quantitatively, the extent of translocation on glass was similar to solution; however, the kinetics was slower. An order of magnitude reduction in the apparent rate constant of translocation was observed on glass compared to solution. This indicates that when the apparatus functions in close proximity to glass, a change occurs in either the rate-limiting step or the features of the step. Future work will be required to deconvolve these possibilities.

The chemomechanical coupling between energy consumed (ATP hydrolyzed) and work done (precursor translocated) only differed twofold on glass when compared to solution. By this metric, coassembled proteoliposomes YEG-A in glass-supported lipid bilayers performed more efficiently (consumed less ATP per residue translocated) than traditional solution assays with the standard reconstituted YEG + A samples that have long been used in the field. The percentage of active

translocons is significantly lower in YEG + A samples (10%) compared to YEG-A (55%), and SecA can continue to hydrolyze ATP nonproductively when engaged with translocation defective SecYEG.³⁶ Hence, one may expect that the chemomechanical coupling of the YEG + A system would be loose.

Glass was shown to be a more suitable surface than mica for translocation. On average, each accessible translocon on glass underwent just under 3 cycles of pOmpA translocation while those on mica underwent <2 cycles. This difference is likely due to the inherent surface roughness of glass. Topographic asperities may lower the effective drag force experienced by the translocating precursor by providing more submembrane space for the polypeptide to occupy. Insights into the submembrane structure of YEG-A adsorbed to SiO₂, a material closely related to glass coverslips, were provided by NR. In summary, precision surface-coupled assays are poised to uncover mechanisms of biochemically active Sec translocases. More generally, translocation activity assays yield valuable quantification of surface-supported lipid bilayer environments.

MATERIALS AND METHODS

Purification of Sec Components. SecYEG was purified from a strain C43 (DE3) suitable for overexpression of membrane protein⁴⁷ harboring a plasmid encoding SecE with a His-tag at the N terminus, SecYC329S, C385S, and SecG.^{36,48} Cells were broken by passage through a French Pressure Cell (5.5×10^7 Pa), and the membranes were isolated by centrifugation and solubilized in dodecyl- β -maltoside (DBM). SecYEG was purified by chromatography using a HisTrap column (GE Healthcare) and stored at -80 °C in 20 mM Tris-Cl (where 1 M = 1 mol/L), pH 8, 0.3 M NaCl, 10% glycerol, 0.6% DBM, and 2 mM DTT. SecA: wild-type SecA was purified as described⁴⁹ with the following modifications. Intact washed cells were incubated on ice for 30 min with 8 mM EDTA to chelate Mg²⁺ in the cell envelope. The cells were pelleted and washed twice to remove the EDTA before being lysed by three cycles of freezing and thawing in the presence of lysozyme. The removal of EDTA before lysis is crucial to prevent the extraction of zinc from SecA. Following centrifugation, SecA was purified from the relevant supernatants by chromatography. SecB was grown as described.⁵⁰ The cells were disrupted using a French Press (5.5×10^7 Pa) and centrifuged for 2 h at 65k rpm (6800 rad/s) using a Type 90 Ti rotor (Beckman, Coulter). The supernatant was loaded onto a QAE column (TosoHaas) and SecB was purified with a gradient of 200–480 mM NaCl in 20 mM TrisCl, 2 mM DTT, pH 7. SecB was eluted around 350 mM NaCl. Concentrations of the proteins were determined spectrophotometrically at 280 nm using coefficients of extinction as follows: SecB tetramer $47\,600\text{ M}^{-1}\text{ cm}^{-1}$; SecA monomer $78\,900\text{ M}^{-1}\text{ cm}^{-1}$; SecYEG $45\,590\text{ M}^{-1}\text{ cm}^{-1}$.

Preparation of Radiolabeled Precursors. pOmpA and pGBP were produced in strain MM52 from plasmids pAL612 and pAL725 carrying the *ompA* gene or the *mglB* gene, respectively. Cells were grown in M9 minimal media supplemented with 19 amino acids (no Leu) and were radiolabeled by addition of ¹⁴C-Leu (PerkinElmer).³⁶

Preparation of Proteoliposomes. Lipids (*E. coli* polar lipid extract, Avanti) in chloroform were blown dry with N₂ and placed in a vacuum chamber overnight. A dry mechanical vacuum pump (XDSS, Edwards) was used to prevent back streaming of oil, a potential contaminant. Dried lipids were suspended in 10 mM Hepes, pH 7.6, 30 mM KAc, 1 mM Mg(Ac)₂. Unilamellar liposomes were prepared by extrusion through membranes (~100 nm pore diameter, LiposoFast, Avestin). To form proteoliposomes, the liposomes were swelled, but not disrupted, using a ratio of detergent to lipids of 4.65 mM DBM to 5 mM lipids.⁵¹ After swelling for 3 h at room temperature, the proteins to be incorporated were added: SecYEG at 5 μ M (the molar ratio of SecYEG to lipid was 1:1000) and for coassembly of SecA (YEG-A), SecA at 5 μ M dimer. Incubation was continued for 1 h at room temperature followed by addition of

BioBeads SM-2 (BioRad) to remove the detergent. The proteoliposomes were isolated by centrifugation at 436 000g, 20 min at 4 °C in a TL100.1 rotor (Beckman). The pellet was suspended in the same buffer and centrifuged again as earlier. The final pellet was suspended to give a concentration of ~10 mM lipid and 10 μ M SecY. The suspension was stored at -80 °C.

Translocase-Activated ATP Hydrolysis Assay. To mimic the sample preparation for AFM measurements, 100 μ L of proteoliposomes YEG-A was incubated on a freshly cleaved mica surface (V1-grade, Ted Pella Inc.) on ice for 1 h in a water saturated environment. The surface was rinsed 10 times with 50 μ L buffer consisting of 10 mM HEPES, 300 mM KAc, 5 mM MgAc₂, pH 7.6. Then, 50 μ L of the solution was removed and replaced with solution containing radioactive ATP (3.3 mM [γ -³²P] ATP, 0.908 nCi/ μ L, PerkinElmer). At predetermined times, a volume of solution above the surface was removed, mixed with 50 mM EDTA to stop the hydrolysis, and spotted on a TLC plate (Millipore Corporation). The plate was developed in 125 mM KH₂PO₄, dried, exposed to a phosphor imaging plate (Fujifilm BAS-MS 2340) in a closed cassette, and then scanned using a phosphor imager (FLA3000). The percent ATP hydrolyzed was estimated from the proportion of total radioactivity that migrated as inorganic phosphate. To evaluate ATPase activity in solution, the aforementioned procedure was carried out in the absence of the mica incubation and rinsing steps. All experiments were replicated at least three times.

Translocation-Associated ATP Hydrolysis Assay. This assay was carried out in an identical manner to the translocase-activated ATP hydrolysis assay described above with the following modifications. After initial surface incubation of YEG-A and rinsing, 50 μ L of reaction mixture containing precursor protein 1 μ M pOmpA or 1 μ M pGBP, 1 μ M SecB, and 3.3 mM radioactive ATP (3.3 mM [γ -³²P] ATP, 0.908 nCi/ μ L, PerkinElmer) was added to the surface. Immediately following this addition, 30 μ L of the solution above the surface was pipetted out and kept in a separate Eppendorf tube (free solution). At corresponding times, a volume of the membrane-exposed solution or the free solution was mixed with 50 mM EDTA. The remaining analysis was carried as described in the translocase-activated ATP hydrolysis assay.

Translocation Activity Assay. One hundred microliters of proteoliposomes YEG-A were incubated on cleaned glass surfaces (KOH followed by oxygen plasma)¹⁸ or freshly cleaved mica surfaces (V1-grade, Ted Pella) for 1 h on ice in a water-saturated environment. Surfaces were rinsed 10 times with 50 μ L of buffer solution: 10 mM HEPES, 300 mM KAc, 5 mM MgAc₂, pH 7.6. Fifty microliters of radiolabeled precursor mixture, containing 1 μ M pOmpA or 1 μ M pGBP, 1 μ M SecB, 1 μ M SecA, and 3 mM ATP in 10 mM HEPES, 300 mM KAc, 5 mM MgAc, 2 mM DTT, 1 mM EGTA, pH 7.6 buffer was added to the surface in a water-saturated environment at room temperature. At predetermined times, 6 M urea (150 μ L) was added to the surface followed by rinsing (10 mM HEPES, 300 mM KAc, 5 mM MgAc, 2 mM DTT, 1 mM EGTA, pH 7.6) and proteinase K incubation (70 μ L at 19 units/mL for 15 min on ice). The surface was then rinsed 10 times with 100 μ L of buffer: 10 mM HEPES, 300 mM KAc, 5 mM MgAc, 2 mM DTT, 1 mM EGTA, pH 7.6. Approximately 95% of the remaining surface solution was pipetted off. The surface was then dried in the oven at 70 °C for 20 min and exposed to the imaging plate (Fujifilm BAS-MS 2340) in a closed cassette for 48 h. The plate was developed using a GE healthcare Amersham Typhoon. The amount of translocated radioactive precursor was quantified using ImageQuant software. A standard curve was created by spotting known quantities of the radioactive precursor on the surfaces, which were dried and exposed to the imaging plate in a closed cassette for 48 h (identical time to the surface translocation activity assay). The inverse slopes of the curves were used to convert intensity to mol precursor protected. Control experiments were performed in an identical manner described above but in the absence of ATP. Data with borosilicate glass were fit to a single exponential rise to maximum with the equation $y(t) = y_0 + A(1 - e^{-k(t-t_0)})$, where A is the maximal amplitude of the reaction, k is the apparent rate constant, and t_0 corrects for the initial time lag (~15 s). Data with mica were fit to a

line. All experiments were performed at least three times, and standard deviations are shown as error bars.

AFM Imaging. Following previous work,^{12,17} proteoliposomes YEG-A (100 nM in imaging buffer: 10 mM HEPES, 300 mM KAC, 5 mM MgAc, pH 7.6) were incubated for ~30 min at room temperature on freshly cleaved mica to form two-dimensional supported lipid bilayers. To remove the loosely absorbed material, samples were washed three times using 100 μ L of imaging buffer. All AFM images were acquired in imaging buffer in tapping mode using a commercial instrument (Cypher, Asylum Research). BioLever mini tips (BL-AC40TS, Olympus) with measured spring constants ~0.06 N/m were used. Images were recorded at ~32 °C with an estimated tip-sample force <100 pN, deduced by comparing the free space tapping amplitude (~5 nm) to the imaging set point amplitude (~4 nm). The areal density of translocases and translocons was estimated using AFM-measured height thresholds described previously.¹²

Neutron Reflectometry. The NR sample was prepared by chemical vapor deposition of a nominally 100 Å thick dry thermal SiO_x film on a 75 mm diameter, 5 mm thick 100 single crystal silicon wafer N-doped with phosphorus to 1–100 Ω cm. The deposition was performed by exposing the wafer to 14 min of oxygen flow at 15 L per min at 700 °C, using a SandVik model 1314 furnace at the NIST Center for Nanoscale Science and Technology. The sample wafer surface was cleaned by sonicating for 2 min in a saturated ethanolic solution of potassium hydroxide, followed by sonication-assisted rinses with copious 18 M Ω cm reverse osmosis water. YEG-A proteoliposomes were added via a pipette to the pristine SiO_x surface, and droplet spreading was confirmed visually. While still wet, the wafer was mounted in a flow cell so that the SiO_x interface was in contact with a nominally 100 μ m thick reservoir of buffer.

For reflectivity measurements, a monochromatic beam of wavelength 5 Å impinged on the interface between the sample wafer surface and liquid in the 100 μ m thick liquid reservoir. The presample collimating slits were chosen to maintain a constant 50 mm \times 25 mm illuminated interfacial area for each measured angle θ . The postsample collimation was chosen to allow the entire reflected beam to impinge on the detector, which was positioned at an angle 2θ relative to the incoming beam direction to measure specular reflection. Each reflectivity curve covered a range in scattering vector $Q_z = 4\pi\lambda^{-1} \sin(\theta)$ from 0.010 to 0.250 Å⁻¹ with a step size of 0.0024 Å⁻¹.

The reflectivity was calculated as $R = (I(Q_z) - I_B(Q_z))/I_0(Q_z)$, where $I(Q_z)$ is the measured count rate (normalized to a much larger monitor count rate to account for fluctuations in beam intensity). $I_B(Q_z)$ is the background intensity, which arises primarily from incoherent scattering from the liquid reservoir and is calculated by linear interpretation of the intensities measured with the detector positioned at 1.5θ and 2.5θ . $I_0(Q_z)$ is the incident beam intensity (also normalized to the monitor count rate) and is directly measured through the silicon substrate at $\theta = 0$ with the detector positioned in line with the incident beam.

NR data were analyzed using the composition space modeling procedures described previously.⁴¹ Simultaneous optimization of the composition space model for the four buffer conditions was performed on the Bridges^{52,53} high-performance computing system using the DREAM Markov Chain Monte Carlo algorithm⁵⁴ implemented in the software package ReflID.⁵⁵ CI on parameters and model predictions were calculated from parameter distributions derived from 4.1 million DREAM samples after the optimizer had reached steady state.

■ ASSOCIATED CONTENT

● Supporting Information

The Supporting Information is available free of charge on the ACS Publications website at DOI: 10.1021/acs.langmuir.9b01928.

Translocation associated ATP hydrolysis assay on glass surface with pOmpA, comparison of translocation-associated ATP hydrolysis assay on glass and mica

surfaces, translocation activity on mica, standard curves, control experiments evaluate ATP-related changes in lipid bilayer defects, surface topography and roughness comparison between SiO_x and glass surfaces, neutron reflectivity of SecYEG proteoliposomes on SiO_x, and NR fitting data (PDF)

■ AUTHOR INFORMATION

Corresponding Author

*E-mail: kinggm@missouri.edu.

ORCID

David P. Hoogerheide: 0000-0003-2918-1469

Gavin M. King: 0000-0002-5811-7012

Notes

The authors declare no competing financial interest.

■ ACKNOWLEDGMENTS

The authors gratefully acknowledge discussions with Priya Bariya as well as Angela Lilly for construction of plasmids and Yuying Suo for purification of proteins. This work was supported by the University of Missouri (MU) Research Board, the National Science Foundation CAREER Award #: 1054832 (to G.M.K.), the National Institutes of Health grant GM29798 (to L.L.R.), and an endowment from the Hugo Wurdack Trust at MU. We also acknowledge Peter Litwinowicz at the Center for Nanoscale Science and Technology at the National Institute of Standards and Technology, U.S. Department of Commerce, for performing the thermal oxide film deposition. This work used the Extreme Science and Engineering Discovery Environment (XSEDE), which is supported by National Science Foundation grant number ACI-1053575. Specifically, it used the Bridges system, which is supported by NSF award number ACI-1445606, at the Pittsburgh Supercomputing Center (PSC). Certain commercial materials, equipment, and instruments are identified in this work to describe the experimental procedure as completely as possible. In no case does such an identification imply a recommendation or endorsement by NIST nor does it imply that the materials, equipment, or instruments identified are necessarily the best available for the purpose.

■ REFERENCES

- (1) Tsigotaki, A.; De Geyter, J.; Šoštarić, N.; Economou, A.; Karamanou, S. Protein export through the bacterial Sec pathway. *Nat. Rev. Microbiol.* **2017**, *15*, 21–36.
- (2) Crane, J. M.; Randall, L. L. The Sec System: Protein Export in *Escherichia coli*. *EcoSal Plus* **2017**; DOI: 10.1128/ecosalplus.0002-2017.
- (3) Randall, L. L.; Hardy, S. J. S. Correlation of competence for export with lack of tertiary structure of the mature species: a study in vivo of maltose-binding protein in *E. coli*. *Cell* **1986**, *46*, 921–928.
- (4) Allen, W. J.; Corey, R. A.; Oatley, P.; Sessions, R. B.; Baldwin, S. A.; Radford, S. E.; Tuma, R.; Collinson, I. Two-way communication between SecY and SecA suggests a Brownian ratchet mechanism for protein translocation. *eLife* **2016**, *5*, No. e15598.
- (5) Bauer, B. W.; Shemesh, T.; Chen, Y.; Rapoport, T. A. A “Push and Slide” Mechanism Allows Sequence-Insensitive Translocation of Secretory Proteins by the SecA ATPase. *Cell* **2014**, *157*, 1416–1429.
- (6) Kedrov, A.; Kusters, I.; Driessen, A. J. M. Single-molecule studies of bacterial protein translocation. *Biochemistry* **2013**, *52*, 6740–6754.

- (7) Sanganna Gari, R. R.; Frey, N. C.; Mao, C.; Randall, L. L.; King, G. M. Dynamic Structure of the Translocon SecYEG in Membrane. *J. Biol. Chem.* **2013**, *288*, 16848–16854.
- (8) Koch, S.; de Wit, J. G.; Vos, I.; Birkner, J. P.; Gordiichuk, P.; Herrmann, A.; van Oijen, A. M.; Driessen, A. J. M. Lipids Activate SecA for High Affinity Binding to the SecYEG Complex. *J. Biol. Chem.* **2016**, *291*, 22534–22543.
- (9) Fessl, T.; Watkins, D.; Oatley, P.; Allen, W. J.; Corey, R. A.; Horne, J.; Baldwin, S. A.; Radford, S. E.; Collinson, I.; Tuma, R. Dynamic action of the Sec machinery during initiation, protein translocation and termination. *eLife* **2018**, *7*, No. e35112.
- (10) Chada, N.; Chattrakun, K.; Marsh, B. P.; Mao, C.; Bariya, P.; King, G. M. Single-molecule observation of nucleotide induced conformational changes in basal SecA-ATP hydrolysis. *Sci. Adv.* **2018**, *4*, No. eaat8797.
- (11) Catipovic, M. A.; Bauer, B. W.; Loparo, J. J.; Rapoport, T. A. Protein translocation by the SecA ATPase occurs by a power-stroke mechanism. *EMBO J.* **2019**, *38*, No. e101140.
- (12) Sanganna Gari, R. R.; Chattrakun, K.; Marsh, B. P.; Mao, C.; Chada, N.; Randall, L. L.; King, G. M. Direct visualization of the E. coli Sec translocase engaging precursor proteins in lipid bilayers. *Sci. Adv.* **2019**, *5*, No. eaav9404.
- (13) Vandenberk, N.; Karamanou, S.; Portaliou, A. G.; Zorzini, V.; Hofkens, J.; Hendrix, J.; Economou, A. The Preprotein Binding Domain of SecA Displays Intrinsic Rotational Dynamics. *Structure* **2019**, *27*, 90.
- (14) Seinen, A.-B.; Driessen, A. J. M. Single-Molecule Studies on the Protein Translocon. *Annu. Rev. Biophys.* **2019**, *48*, 185–207.
- (15) Serdiuk, T.; Steudle, A.; Mari, S. A.; Manioglou, S.; Kaback, H. R.; Kuhn, A.; Müller, D. J. Insertion and folding pathways of single membrane proteins guided by translocases and insertases. *Sci. Adv.* **2019**, *5*, No. eaau6824.
- (16) Bippes, C. A.; Muller, D. J. High-resolution atomic force microscopy and spectroscopy of native membrane proteins. *Rep. Prog. Phys.* **2011**, *74*, 086601.
- (17) Mao, C.; Cheadle, C. E.; Hardy, S. J. S.; Lilly, A. A.; Suo, Y.; Sanganna Gari, R. R.; King, G. M.; Randall, L. L. Stoichiometry of SecYEG in the active translocase of Escherichia coli varies with precursor species. *Proc. Natl. Acad. Sci. U.S.A.* **2013**, *110*, 11815–11820.
- (18) Chada, N.; Sigdel, K. P.; Sanganna Gari, R. R.; Matin, T. R.; Randall, L. L.; King, G. M. Glass is a Viable Substrate for Precision Force Microscopy of Membrane Proteins. *Sci. Rep.* **2015**, *5*, 12550.
- (19) Tamm, L. K.; McConnell, H. M. Supported phospholipid bilayers. *Biophys. J.* **1985**, *47*, 105–113.
- (20) Castellana, E. T.; Cremer, P. S. Solid supported lipid bilayers: From biophysical studies to sensor design. *Surf. Sci. Rep.* **2006**, *61*, 429–444.
- (21) Karner, A.; Nimmervoll, B.; Plochberger, B.; Klotzsch, E.; Horner, A.; Knyazev, D. G.; Kuttner, R.; Winkler, K.; Winter, L.; Siligan, C.; Ollinger, N.; Pohl, P.; Preiner, J. Tuning membrane protein mobility by confinement into nanodomains. *Nat. Nanotechnol.* **2017**, *12*, 260.
- (22) Glazier, R.; Salaita, K. Supported lipid bilayer platforms to probe cell mechanobiology. *Biochim. Biophys. Acta, Biomembr.* **2017**, *1859*, 1465–1482.
- (23) Perkins, T. T. Optical traps for single molecule biophysics: a primer. *Laser Photonics Rev.* **2009**, *3*, 203–220.
- (24) Radmacher, M.; Fritz, M.; Hansma, H.; Hansma, P. Direct observation of enzyme activity with the atomic force microscope. *Science* **1994**, *265*, 1577–1579.
- (25) Bezanilla, M.; Drake, B.; Nudler, E.; Kashlev, M.; Hansma, P. K.; Hansma, H. G. Motion and enzymatic degradation of DNA in the atomic force microscope. *Biophys. J.* **1994**, *67*, 2454–2459.
- (26) Viani, M. B.; Pietrasanta, L. I.; Thompson, J. B.; Chand, A.; Gebeshuber, I. C.; Kindt, J. H.; Richter, M.; Hansma, H. G.; Hansma, P. K. Probing protein-protein interactions in real time. *Nat. Struct. Biol.* **2000**, *7*, 644–647.
- (27) Nakanishi, K.; Sakiyama, T.; Imamura, K. On the adsorption of proteins on solid surfaces, a common but very complicated phenomenon. *J. Biosci. Bioeng.* **2001**, *91*, 233–244.
- (28) Kranz, C.; Kueng, A.; Lugstein, A.; Bertagnolli, E.; Mizaikoff, B. Mapping of enzyme activity by detection of enzymatic products during AFM imaging with integrated SECM-AFM probes. *Ultra-microscopy* **2004**, *100*, 127–134.
- (29) Schaap, I. A. T.; Carrasco, C.; de Pablo, P. J.; Schmidt, C. F. Kinesin walks the line: single motors observed by atomic force microscopy. *Biophys. J.* **2011**, *100*, 2450–2456.
- (30) Kodera, N.; Yamamoto, D.; Ishikawa, R.; Ando, T. Video imaging of walking myosin V by high-speed atomic force microscopy. *Nature* **2010**, *468*, 72–76.
- (31) Ando, T.; Uchihashi, T.; Scheuring, S. Filming biomolecular processes by high-speed atomic force microscopy. *Chem. Rev.* **2014**, *114*, 3120–3188.
- (32) Arredondo, M.; Stoytcheva, M.; Morales-Reyes, I.; Batina, N. AFM and MFM techniques for enzyme activity imaging and quantification. *Biotechnol. Biotechnol. Equip.* **2018**, *32*, 1065–1074.
- (33) Nievergelt, A. P.; Banterle, N.; Andany, S. H.; Gönczy, P.; Fantner, G. E. High-speed photothermal off-resonance atomic force microscopy reveals assembly routes of centriolar scaffold protein SAS-6. *Nat. Nanotechnol.* **2018**, *13*, 696–701.
- (34) Mao, C.; Hardy, S. J. S.; Randall, L. L. Maximal efficiency of coupling between ATP hydrolysis and translocation of polypeptides mediated by SecB requires two protomers of SecA. *J. Bacteriol.* **2009**, *191*, 978–984.
- (35) Krueger, S.; Meuse, C. W.; Majkrzak, C. F.; Dura, J. A.; Berk, N. F.; Tarek, M.; Plant, A. L. Investigation of hybrid bilayer membranes with neutron reflectometry: Probing the interactions of melittin. *Langmuir* **2001**, *17*, 511–521.
- (36) Bariya, P.; Randall, L. L. Coassembly of SecYEG and SecA Fully Restores the Properties of the Native Translocon. *J. Bacteriol.* **2019**, *201*, No. e00493.
- (37) Robson, A.; Gold, V. A. M.; Hodson, S.; Clarke, A. R.; Collinson, I. Energy transduction in protein transport and the ATP hydrolytic cycle of SecA. *Proc. Natl. Acad. Sci. U.S.A.* **2009**, *106*, 5111–5116.
- (38) Lill, R.; Dowhan, W.; Wickner, W. The Atpase Activity of SecA Is Regulated by Acidic Phospholipids, SecY, and the Leader and Mature Domains of Precursor Proteins. *Cell* **1990**, *60*, 271–280.
- (39) Economou, A.; Wickner, W. SecA Promotes Preprotein Translocation by Undergoing Atp-Driven Cycles of Membrane Insertion and Deinsertion. *Cell* **1994**, *78*, 835–843.
- (40) Brundage, L.; Hendrick, J. P.; Schiebel, E.; Driessen, A. J. M.; Wickner, W. The purified E. coli integral membrane protein SecYE is sufficient for reconstitution of SecA-dependent precursor protein translocation. *Cell* **1990**, *62*, 649–657.
- (41) Shekhar, P.; Nanda, H.; Lösche, M.; Heinrich, F. Continuous distribution model for the investigation of complex molecular architectures near interfaces with scattering techniques. *J. Appl. Phys.* **2011**, *110*, 102216–10221612.
- (42) Zimmer, J.; Nam, Y.; Rapoport, T. A. Structure of a complex of the ATPase SecA and the protein-translocation channel. *Nature* **2008**, *455*, 936.
- (43) Majkrzak, C. F.; Metting, C.; Maranville, B. B.; Dura, J. A.; Satija, S.; Udovic, T.; Berk, N. F. Determination of the effective transverse coherence of the neutron wave packet as employed in reflectivity investigations of condensed-matter structures. I. Measurements. *Phys. Rev. A* **2014**, *89*, 033851.
- (44) Carrion-Vazquez, M.; Oberhauser, A. F.; Fowler, S. B.; Marszalek, P. E.; Broedel, S. E.; Clarke, J.; Fernandez, J. M. Mechanical and chemical unfolding of a single protein: A comparison. *Proc. Natl. Acad. Sci. U.S.A.* **1999**, *96*, 3694–3699.
- (45) Kohn, J. E.; Millett, I. S.; Jacob, J.; Zagrovic, B.; Dillon, T. M.; Cingel, N.; Dothager, R. S.; Seifert, S.; Thiyagarajan, P.; Sosnick, T. R.; Hasan, M. Z.; Pande, V. S.; Ruczinski, I.; Doniach, S.; Plaxco, K. W. Random-coil behavior and the dimensions of chemically unfolded proteins. *Proc. Natl. Acad. Sci. U.S.A.* **2004**, *101*, 12491–12496.

(46) Cremer, P. S.; Boxer, S. G. Formation and spreading of lipid bilayers on planar glass supports. *J. Phys. Chem. B* **1999**, *103*, 2554–2559.

(47) Miroux, B.; Walker, J. E. Over-production of Proteins in *Escherichia coli*: Mutant Hosts that Allow Synthesis of some Membrane Proteins and Globular Proteins at High Levels. *J. Mol. Biol.* **1996**, *260*, 289–298.

(48) Cannon, K. S.; Or, E.; Clemons, W. M.; Shibata, Y.; Rapoport, T. A. Disulfide bridge formation between SecY and a translocating polypeptide localizes the translocation pore to the center of SecY. *J. Cell Biol.* **2005**, *169*, 219–225.

(49) Randall, L. L.; Crane, J. M.; Lilly, A. A.; Liu, G.; Mao, C.; Patel, C. N.; Hardy, S. J. S. Asymmetric binding between SecA and SecB two symmetric proteins: implications for function in export. *J. Mol. Biol.* **2005**, *348*, 479–489.

(50) Randall, L. L.; Topping, T. B.; Smith, V. F.; Diamond, D. L.; Hardy, S. J. S. [35] SeeB: A chaperone from *Escherichia coli*. *Methods Enzymol.* **1998**, *290*, 444.

(51) Lambert, O.; Levy, D.; Ranck, J.-L.; Leblanc, G.; Rigaud, J.-L. A new “gel-like” phase in dodecyl maltoside–lipid mixtures: implications in solubilization and reconstitution studies. *Biophys. J.* **1998**, *74*, 918–930.

(52) Nystrom, N. A.; Levine, M. J.; Roskies, R. Z.; Scott, J. R. Bridges. In *Proceedings of the 2015 XSEDE Conference on Scientific Advancements Enabled by Enhanced Cyberinfrastructure-XSEDE'15*; ACM: St. Louis, Missouri, 2015; pp 1–8.

(53) Towns, J.; Cockerill, T.; Dahan, M.; Foster, I.; Gaither, K.; Grimshaw, A.; Hazlewood, V.; Lathrop, S.; Lifka, D.; Peterson, G. D.; Roskies, R.; Scott, J. R.; Wilkins-Diehr, N. XSEDE: Accelerating Scientific Discovery. *Comput. Sci. Eng.* **2014**, *16*, 62–74.

(54) Vrugt, J. A.; ter Braak, C. J. F.; Diks, C. G. H.; Robinson, B. A.; Hyman, J. M.; Higdon, D. Accelerating Markov Chain Monte Carlo Simulation by Differential Evolution with Self-Adaptive Randomized Subspace Sampling. *Int. J. Nonlinear Sci. Numer. Simul.* **2009**, *10*, 273–290.

(55) Kienzle, P. A.; Krycka, J.; Patel, N.; Metting, C.; Sahin, I.; Fu, Z.; Chen, W.; Mont, A.; Tighe, D. *ReflID*, version 0.7.7 [Computer Software]; University of Maryland: College Park, MD, 2016.

Supporting Information

Protein Translocation Activity in Surface-Supported Lipid Bilayers

*Kanokporn Chattrakun¹, David P. Hoogerheide², Chunfeng Mao³, Linda L. Randall³, and
Gavin M. King^{1,3,*}*

¹ Department of Physics and Astronomy, University of Missouri-Columbia, Columbia, MO 65211, USA.

² Center for Neutron Research, National Institute of Standards and Technology, Gaithersburg, MD, 20899, USA.

³ Department of Biochemistry, University of Missouri-Columbia, Columbia, MO 65211, USA.

*Corresponding author, email: kinggm@missouri.edu

This document contains:

Figure S1. Translocation associated ATP hydrolysis assay on glass surface with pOmpA.
Figure S2. Comparison of translocation associated ATP hydrolysis assay on glass and mica surfaces.
Figure S3. Translocation activity on mica.
Figure S4. Standard curves.
Figure S5. Control experiments evaluate ATP-related changes in lipid bilayer defects.
Figure S6. Surface topography and roughness comparison between SiO_x and borosilicate glass surfaces.
Figure S7. Neutron reflectivity of proteoliposomes YEG·A on SiO_x surfaces.
Table S1. Neutron reflectometry fitting data.

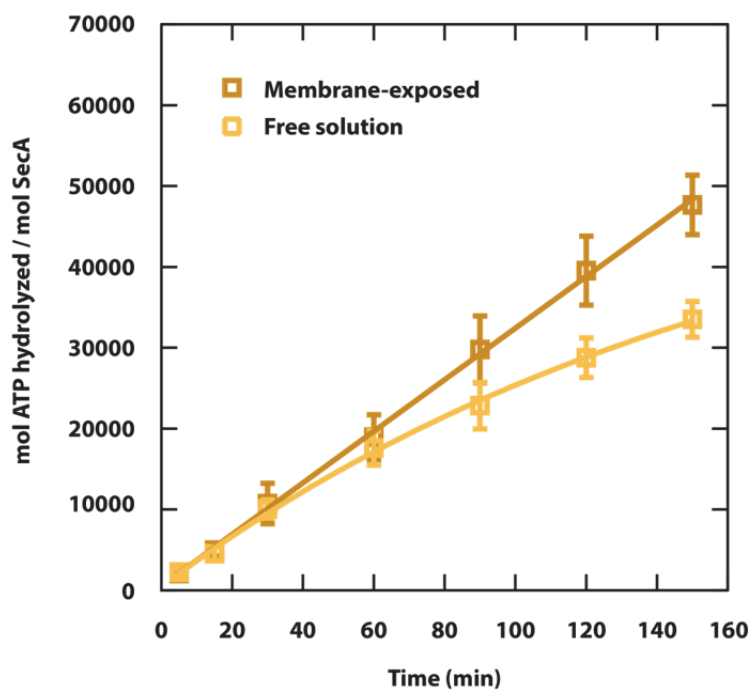


Figure S1. Translocation associated ATP hydrolysis assay on glass surface with pOmpA. Proteoliposomes YEG-A were deposited on freshly cleaned borosilicate glass coverslips. ATPase activity was assessed in the presence of pOmpA and SecB for membrane-exposed volumes (dark brown squares) and free solution (light brown squares). Error bars are SD, $N=3$.

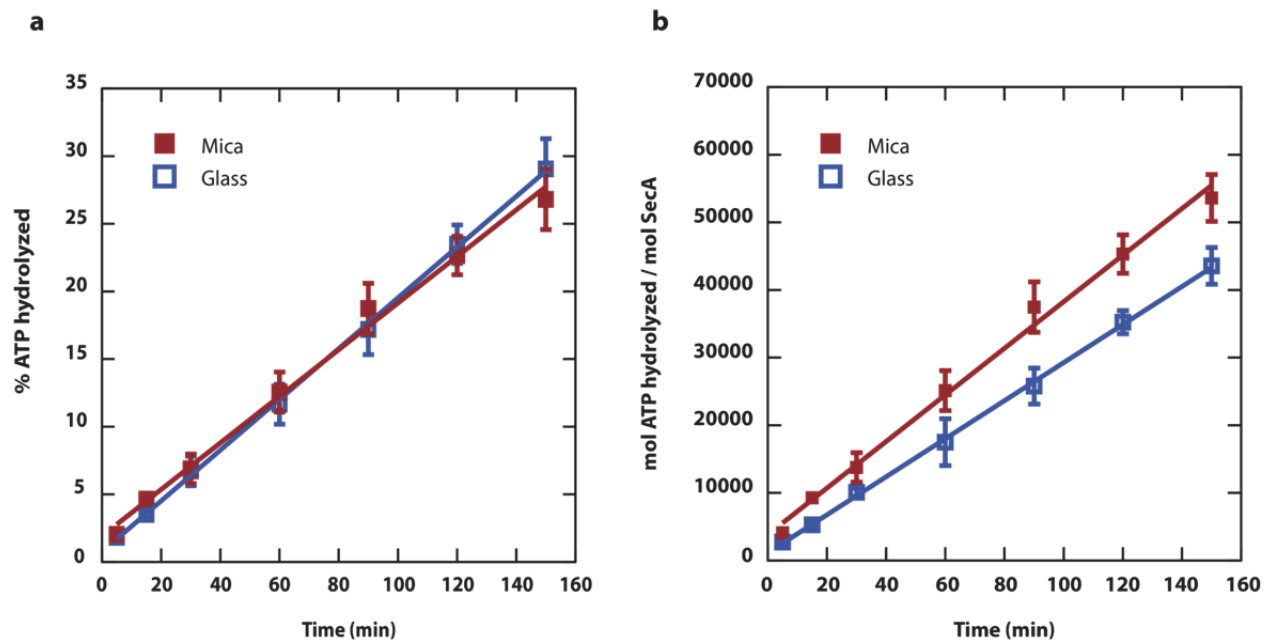


Figure S2. Comparison of translocation associated ATP hydrolysis assay on glass and mica surfaces. Proteoliposomes YEG·A were deposited on either freshly cleaned borosilicate glass coverslips or freshly cleaved mica. ATPase activity was assessed in the presence of pGBP and SecB. **(a)** The percent ATP hydrolyzed versus time from the membrane-exposed volume is shown: glass (blue open squares); mica (red closed squares). **(b)** Plots of the data after conversion to mol ATP hydrolyzed and normalization to the estimated amount of SecA available. Error bars are SD, $N=3$.

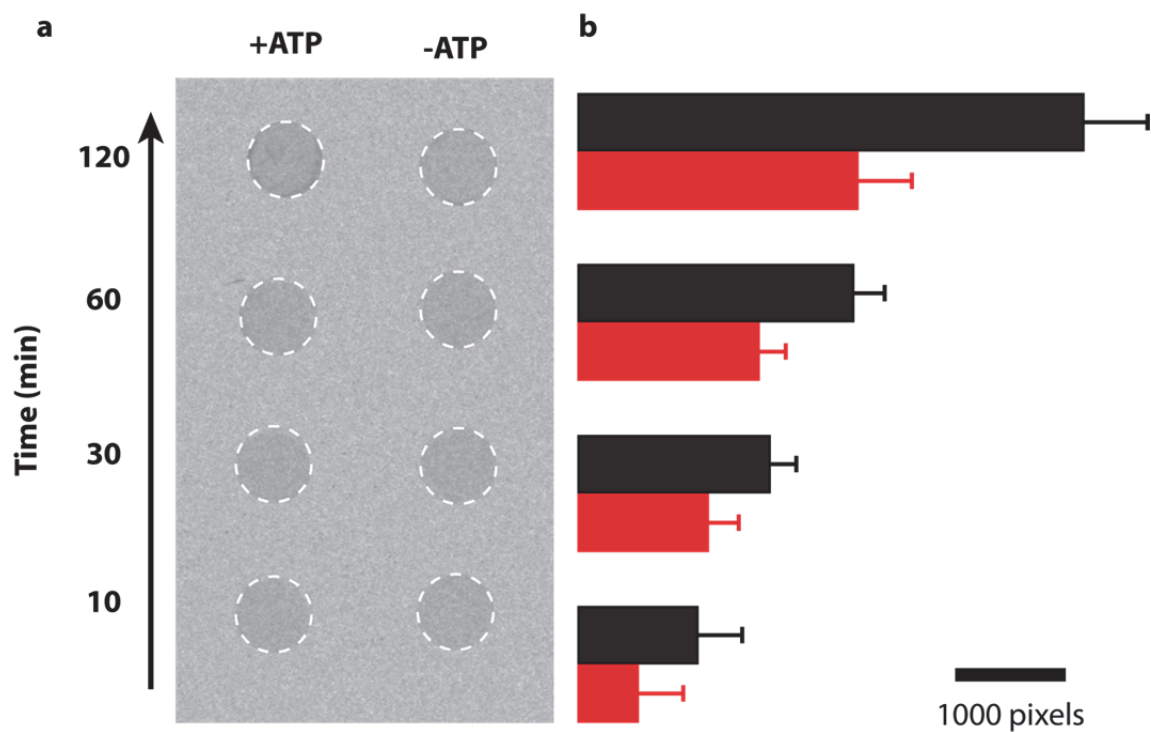


Figure S3. Translocation activity on mica. Translocation activity assays were performed on mica in the same manner as described for glass. **(a)** Phosphor image data for pOmpA on mica. Dashed circles highlight the area of each mica disk. **(b)** Bar graphs represent the integrated intensity of pixels inside the dashed circles at corresponding time points (black = +ATP, red = -ATP). Error bars are SD, $N=3$.

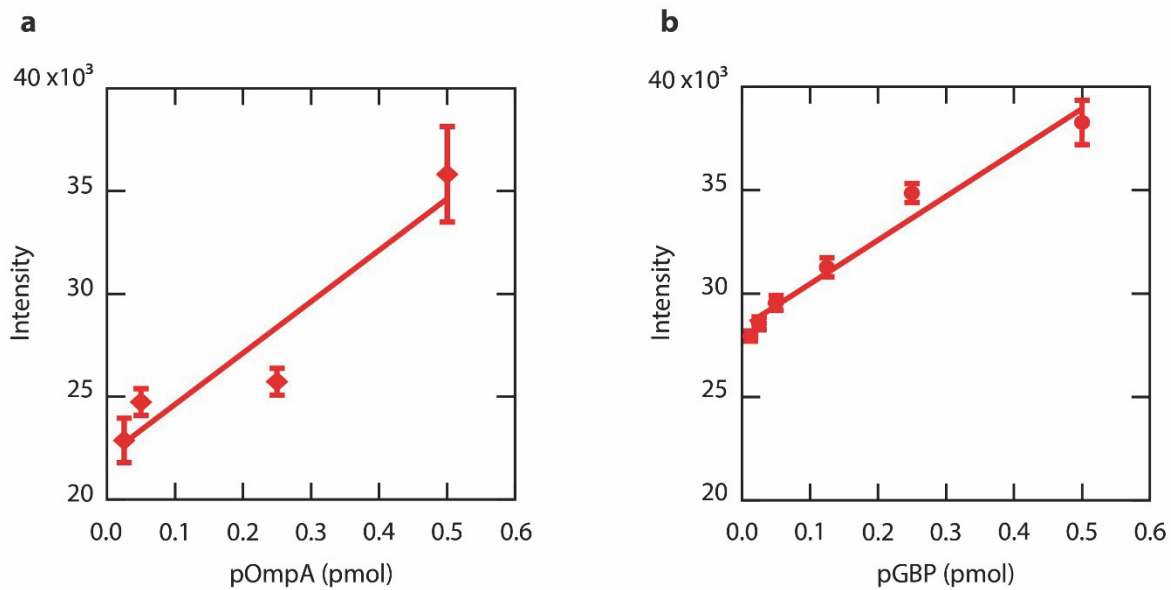


Figure S4. Standard curves. Calibration curves used to convert intensity of the phosphor image to pmol precursor protected. (a) Shows a standard curve for pOmpA, (b) for pGBP. Lines were used to fit the intensity as a function of concentration. Surfaces prepared for standard curves were placed in the same cassette as those from the translocation activity experiments. Therefore, all surfaces were subjected to the same background. Error bars are SD, $N=3$.

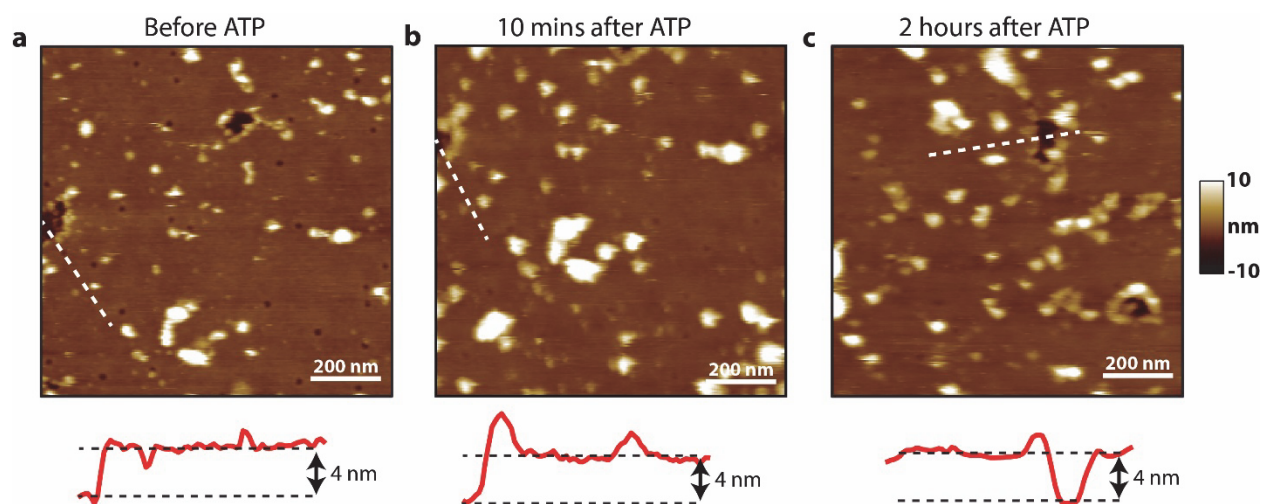


Figure S5. Control experiments evaluate ATP-related changes in lipid bilayer defects. Representative AFM images of proteoliposomes YEG·A on glass surfaces (a) before, (b) 10 minutes after, and (c) two hours after adding 3 mM ATP into the imaging buffer. The same location of the lipid bilayer surface (with an offset) is shown in (a) and (b). (c) Shows a different area of the bilayer. The line scans (red, location in image: white dashed) below each image indicate the height of the lipid bilayer (4 nm) remains unchanged. Overall, the data suggest that the addition of ATP does not grossly alter the bilayer defects.

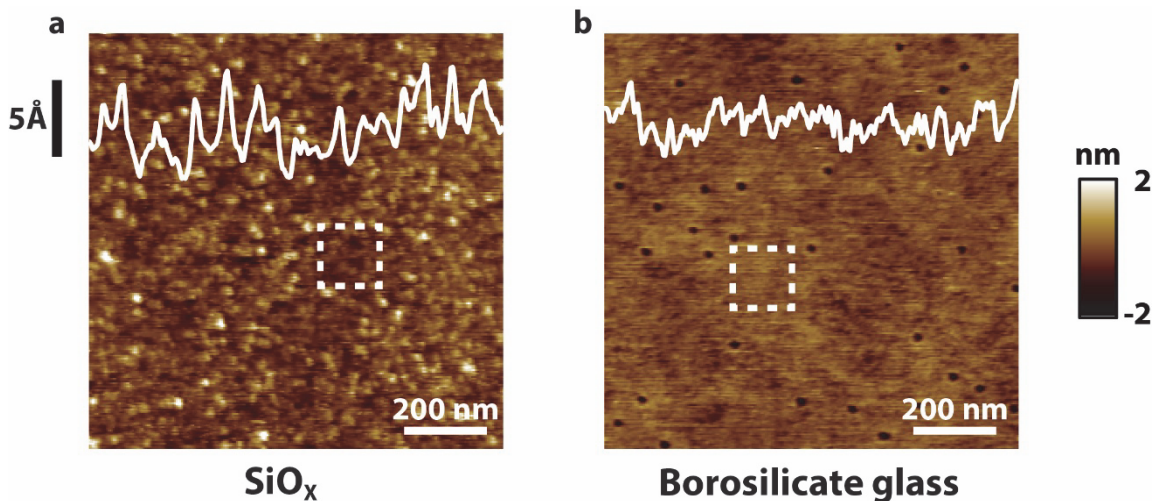


Figure S6. Surface topography and roughness comparison between SiO_x and borosilicate glass surfaces. Representative AFM images of SiO_x and borosilicate glass coverslips are shown in (a) and (b), respectively. Line scans (white, with 5 Å vertical scale bar) are overlaid. Prior to imaging, both surfaces were sonicated in KOH saturated ethanol for 2 minutes. The borosilicate glass was further treated in an oxygen plasma for 10 minutes as described.¹ Immediately after cleaning, imaging buffer was added and AFM images were acquired. Representative areas of 150 x 150 nm² were used to characterize the roughness of the surfaces identified by dashed white squares in (a) and (b). The RMS roughness values were 2.5 Å and 1.7 Å for the SiO_x and borosilicate glass, respectively. The same identical tip was used to acquire all data. The SiO_x surface was imaged after the borosilicate glass surface. The same identical tip was then used to image borosilicate glass again. The resulting RMS values were similar, indicating that the overall dimensions of the tip (which are convolved into the RMS analysis) were static during the analysis.

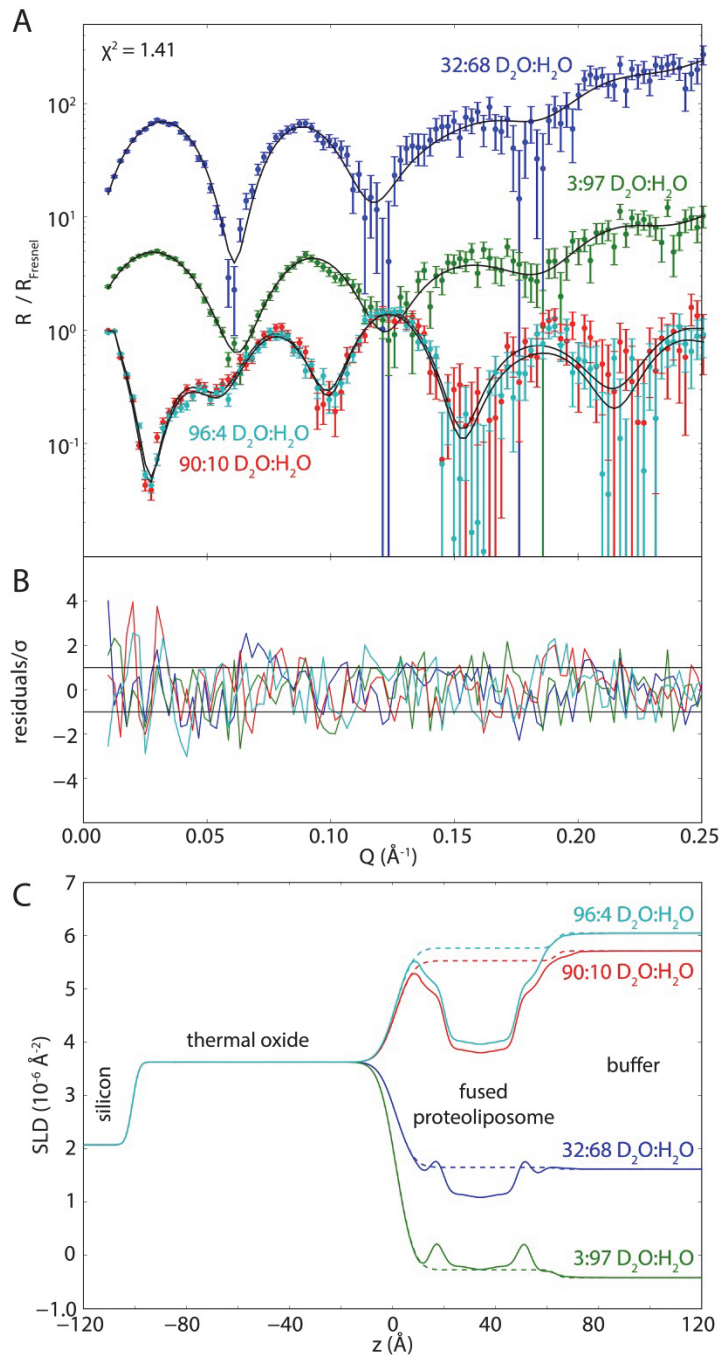


Figure S7. Neutron reflectivity of proteoliposomes YEG·A on SiOx surfaces. (a) Neutron reflectivity in buffers based on D₂O, H₂O, and a 3:7 mixture of D₂O/H₂O. Reflectivity is normalized to the Fresnel reflectivity expected from the interface between silicon and each buffer. Error bars represent 68% confidence intervals arising from Poisson counting uncertainty. (b) Residuals of volume occupancy model optimization to reflectivity curves. (c) SLD profiles derived from the optimized volume occupancy model. Solid and dashed lines show the SLD profiles of two incoherently added models corresponding to surface regions with and without adsorbed proteoliposomes, respectively.

Table S1. Neutron reflectometry fitting data. List of fit parameters with optimization limits and optimized values with confidence intervals (CI).

Parameter (units)	Lower bound	Upper bound	Mean value	Lower 68% CI	Upper 68% CI
<i>Beam parameters</i>					
Total reflectance	0.9	1.05	0.983	0.977	0.988
Sample broadening factor	0.1	4.0	0.16	0.12	0.25
Angle misalignment (°)	-0.005	0.005	0.0014	-0.0014	0.0040
<i>Bulk parameters</i>					
SLD of first data set (10^{-6} \AA^{-2})	4.0	6.4	5.66	5.59	5.72
SLD of second data set (10^{-6} \AA^{-2})	-0.566	2.4	1.65	1.60	1.69
SLD of third data set (10^{-6} \AA^{-2})	4.0	6.4	5.99	5.92	6.05
SLD of fourth data set (10^{-6} \AA^{-2})	-0.566	2.4	-0.33	-0.41	-0.26
Background of first data set (10^{-6})	-10	100	0.30	0.23	0.37
Background of second data set (10^{-6})	-10	100	1.98	1.89	2.08
Background of third data set (10^{-6})	-10	100	0.18	0.11	0.24
Background of fourth data set (10^{-6})	-10	100	2.34	2.18	2.50
<i>Substrate parameters</i>					
Si/SiO _x rms interfacial roughness (Å)	2	15	2.19	2.05	2.45
SiO _x thickness (Å)	70	110	102.62	102.38	102.85
SiO _x SLD (10^{-6} \AA^{-2})	2.4	4.4	3.618	3.598	3.639
SiO _x rms surface roughness (Å)	2	25	4.53	3.99	5.00
<i>Bilayer parameters</i>					
Substrate- headgroup separation (Å)	-5	50	9.10	8.66	9.58
Acyl chain length per leaflet (Å)	10	25	13.25	12.85	13.72
Volume fraction of bilayer	0	1	0.278	0.269	0.287
Volume fraction of peripheral protein	0	0.4	0.06	0.01	0.22
Length of peripheral protein (Å)	10	80	15.5	10.6	72.2
Volume fraction of peripheral protein after rinsing	0	0.4	0.03	0.01	0.08
<i>Nonspecific adsorption parameters</i>					
Volume fraction of nonspecifically adsorbed protein	0	0.4	0.056	0.045	0.067
Length of nonspecifically adsorbed protein (Å)	10	80	57.5	53.4	60.3
Volume fraction of nonspecifically adsorbed protein after rinsing	0	0.4	0.065	0.055	0.074
Fraction of surface described only by nonspecific adsorption	0	1	0.43	0.40	0.45

References cited

1. Chada, N.; Sigdel, K. P.; Sanganna Gari, R. R.; Matin, T. R.; Randall, L. L.; King, G. M. *Sci Rep* **2015**, *5*, 12550.